Intense isolated attosecond pulse generation from relativistic laser plasmas using few-cycle laser pulses

Guangjin Ma,[1,2,a)] William Dallari,[2] Antonin Borot,[2] Ferenc Krausz,[2,3] Wei Yu,[1] George D. Tsakiris,[2] and Laszlo Veisz[2]
[1]*State Key Laboratory of High Field Laser Physics, Shanghai Institute of Optics and Fine Mechanics, Chinese Academy of Sciences, Shanghai 201800, China*
[2]*Max-Planck-Institut für Quantenoptik, D-85748 Garching, Germany*
[3]*Department für Physik, Ludwig-Maximilians-Universität, D-85748 Garching, Germany*

(Received 13 November 2014; accepted 18 February 2015; published online 6 March 2015)

We have performed a systematic study through particle-in-cell simulations to investigate the generation of attosecond pulse from relativistic laser plasmas when laser pulse duration approaches the few-cycle regime. A significant enhancement of attosecond pulse energy has been found to depend on laser pulse duration, carrier envelope phase, and plasma scale length. Based on the results obtained in this work, the potential of attaining isolated attosecond pulses with $\sim$100 μJ energy for photons $>$16 eV using state-of-the-art laser technology appears to be within reach. © *2015 AIP Publishing LLC*. [http://dx.doi.org/10.1063/1.4914087]

I. INTRODUCTION

The prodigious progress in laser technology has made readily available laser systems delivering pulses of a few-cycle duration at high repetition rate.[1–4] Further innovations have led to successful amplification of these pulses up to 100-mJ level with simultaneous control or characterization over some crucial laser pulse parameters produced by such systems, e.g., contrast level[4] or carrier-envelope phase.[5] These advancements have enabled the generation of enormous peak intensities in the laboratory reaching the 10^{20} W/cm^2 level. As a consequence, the road to whole new areas of research in high field physics has been opened.

One such area of great interest is the efficient frequency up-conversion of the laser light into harmonics. The significance of this process is ultimately linked to the generation of energetic attosecond bursts (attosecond pulses or APs) for extreme ultraviolet (XUV) photons and their impact to the emerging field of attosecond science.[6] To date, most of the AP sources are based on high-order harmonic generation (HHG) in gaseous media.[7–14] They display, however, limited brightness[15,16] due to the fact that the harmonic generation process in atoms exhibits a saturation intensity over which the conversion efficiency drops due to medium depletion. This severely restricts the scope of applications, since the availability of a source delivering rather intense APs is the prerequisite for XUV-pump-XUV-probe spectroscopy. To circumvent this limitation, AP source from relativistic interaction of an intense laser pulse with overdense plasma has been suggested.[17–19] The main advantage over the process of harmonic generation in atomic medium is that the plasma medium allows the use of higher laser intensities available from state-of-the-art multi-TW and PW laser systems, thus rendering them the ideal drivers to a source of intense AP trains.

To date, three distinct mechanisms have been identified as giving rise to HHG in the interaction of intense laser pulses with solid density plasma: the coherent wake emission (CWE),[20] the relativistically oscillating mirror (ROM),[21] and the coherent synchrotron emission (CSE)[22] mechanism. All of them are associated with dense energetic electron populations driven coherently at solid density plasma surfaces. However, they involve fundamentally different energy coupling processes, and each of them has its own dominant parameter regime and spectral signature. An important role in the delimitation between the various mechanisms plays the normalized vector potential a_L value associated with the incident laser pulse, which in terms of the focused laser intensity I_L and laser wavelength λ_L is given by $a_L^2 = I_L\lambda_L^2/[1.38\times10^{18}\,\mathrm{W\,cm^{-2}\,\mu m^2}]$. However, a number of other parameters associated with the interaction may also play a decisive role in determining which mechanism prevails. The most important are the plasma scale length L, the carrier envelope phase (CEP) φ_{CEP} (especially for few-cycle laser pulses), and the geometry (angle of incidence of the laser pulse). Briefly, the main characteristics of each process are as follows: In the CWE process, the collectively moving electrons reenter the plasma-vacuum interface and bunch into high dense electron jets in the overdense plasma region where they excite collective electrostatic oscillations. Due to the strong density inhomogeneity, the electrostatic oscillations then couple back to electromagnetic modes through linear mode conversion and thus generate harmonics. CWE is the predominant mechanism when the normalized laser intensity parameter is weakly relativistic, i.e., $a_L \lesssim 1$, and plasma scale length is short, e.g., $L \sim 0.01\lambda_L$. The CWE spectra feature a cut-off at the plasma frequency corresponding to the highest plasma density. In the ROM process, the harmonic emission is attributed to Doppler upshift of the reflected laser field on relativistically moving electrons pulled out of plasma during a laser cycle. The process is dominant for $a_L \gg 1$, although there are also reports at lower intensities[23] when plasma scale lengths are about $L \sim 0.1\lambda_L$. The harmonic orders from this mechanism extend beyond

a)Electronic mail: guangjin.ma@mpq.mpg.de

the plasma cut-off frequency and display a well-known −8/3 spectral efficiency scaling.[24] Finally, in the same intensity range where the ROM mechanism is present but when laser and plasma evolution are matched in a certain way, highly dense electron nanobunches can be formed that co-propagate with the laser wavefront. The stored energy in these nanobunches couples efficiently into radiative electromagnetic modes through a process similar to that of the well known synchrotron emission and thus generates harmonics.[22,25–28] This process is called CSE. In addition to the laser intensity and plasma scale length dependence, conditions for CSE harmonics in specular direction have also been mentioned to depend on angle of incidence, laser pulse duration, and carrier envelope phase;[22] although no detailed investigation on the influence of these parameters has been performed. CSE spectra usually feature a shallower spectral efficiency scaling than the ROM spectra, from −8/3 upto −4/3. It appears that for the range of intensities we primarily investigate in this report, the widely accepted ROM mechanism is indeed the relevant process. In some cases, the CSE mechanism also takes place as to enhance higher harmonics, although the parameter regime we are interested in is not yet the optimal to clearly show this mechanism. It should be pointed out here that under certain conditions more than one mechanism can be active. For example, for $a_L \approx 0.7$ and $L \approx 0.03\lambda_L$, the interference fringes between ROM and CWE have been observed around the transition harmonic order,[29] showing the coexistence of both mechanisms.

The purpose of the report is to extend the route proposed by earlier work of Tsakiris *et al.*[18] and investigates in more detail the parameter range for which intense isolated AP can be generated. Also, to examine under what conditions harmonic enhancement due to the CSE mechanism occurs. In this context, the influence of preplasma scale length and carrier envelope phase has been studied simultaneously for laser pulse duration from few up to ten cycles. This is a systematic study based on particle-in-cell (PIC) simulations aiming at determining the optimum path towards the goal of realizing intense isolated AP. For simplicity, we limit ourselves in this report to the discussion of PIC simulation results, and we have to leave more detailed analysis of the energy coupling process and of the parametric dependence to future work.

II. SIMULATION DETAILS

The simulations are performed using the 1D PIC code LPIC++.[21] The incident laser pulse is assumed to have a Gaussian temporal shape and a linear polarization with electric field given by $E_y^{inc} = a_L \exp\{-2\ln 2[\psi/(2\pi\bar{\tau}_L)]^2\} \cos(\psi + \varphi_{CEP})$, where a_L is the normalized laser field, and $\bar{\tau}_L$ the intensity full-width-half-maximum (FWHM) laser pulse duration normalized to the laser period T_L. Throughout this paper, we assume $a_L = 10$, which corresponds to a laser intensity of $2 \times 10^{20}\,\mathrm{W/cm^2}$ for a laser central wavelength λ_L of 800 nm. The density profile of the interacting plasma has an exponential interface layer in front of it with scale length L. It rises from $0.2n_c$ up to a maximum of $90n_c$ and then it is followed by a $2\lambda_L$ thick constant density distribution, with n_c being the critical electron density at the laser wavelength. Although in experiments, higher electron densities are encountered (e.g., in glass targets $400n_c$ when fully ionized), this is permissible because, due to the presence of the interface layer, the interaction takes place primarily near the relativistic critical density $(\sim a_L n_c)$ and thus far away from the maximum plasma density. In addition, with the choice of $90n_c$ instead of $400n_c$ as the maximum plasma density, we can greatly reduce the computation load. Besides, in this case, an aluminum filter window can select all harmonics above the highest plasma frequency, thus precluding the contribution of CWE mechanism. The p-polarized laser pulse is incident onto the plasma layer at an angle α of 45°. In LPIC++, this oblique incidence geometry is transformed into 1D case using the Bourdier technique.[30]

All the simulations presented in this paper are performed with moving ions with very high mass $m/m_e = 50\,000$. The resolution used is 1000 cells per laser wavelength, 1414 time steps per laser cycle. There are 900 particles per cell for both electron and ion species for the highest density of $90n_c$, which means that one particle denotes a density of $0.1n_c$. A simulation box with a total length of $12\lambda_L$ is aligned on x axis from $x = 0\lambda_L$ to $x = 12\lambda_L$. The laser is incident from left to right. The $2\lambda_L$ thick flat top density profile is always located between $x = 9\lambda_L$ and $x = 11\lambda_L$. For the indicated lowest and highest plasma density of the exponential interface layer, it is always cut at a point with a distance of 6 times the plasma scale length away from the point $x = 9\lambda_L$. Thus, even for the worst case of $L = 1\lambda_L$, there is at least a $3\lambda_L$ long vacuum space between the plasma and the box left end. At the two box ends, electromagnetic waves have open boundary conditions while particles have reflecting boundary conditions. The Gaussian laser pulses used for different durations are always truncated at an intensity level ten orders of magnitude lower than the peak laser intensity. Selected cases for the results presented in this paper have been verified by using higher spatio-temporal resolution, more particles per cell, larger vacuum spaces between plasma and the two box ends, as well as the maximum plasma density as high as $400n_c$; and no clear discrepancies have been found.

The outline of this report is as follows: first, we use a specific case to illustrate the temporal and spectral characteristics of the fields for a typical interaction scenario and a two-cycle laser pulse driver. In what follows, we investigate the optimum conditions for maximum enhancement of attosecond pulse generation (APG). This investigation is based on a quantitative analysis of the HHG yield for a range of the parameters φ_{CEP}, L, and τ_L, corresponding to different interaction conditions. Finally, we discuss the feasibility of realizing an intense single AP using a currently existing sub-5 fs laser system.

III. A TYPICAL INTERACTION SCENARIO

In Fig. 1, the incident laser pulse (blue curve in (a)) has a duration τ_L of 5 fs and CEP φ_{CEP} of 0.75π. It interacts with a plasma layer with scale length L of $0.2\lambda_L$. The reflected electric field is strongly modulated at four temporal positions (red curve in (a)). This enormously broadens the incident spectrum ($I_{inc}(\omega)$ blue curve in (c)) to several hundredth harmonic of

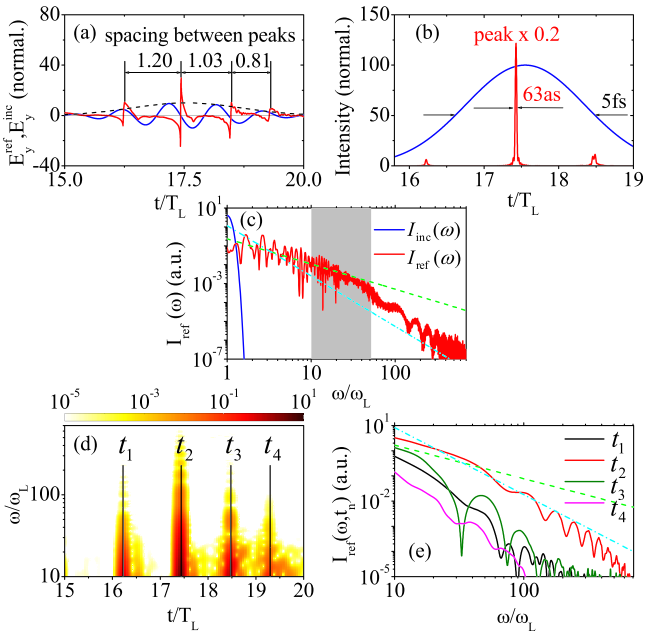

FIG. 1. (a) Reflected (red) and the corresponding incident (blue) laser electric field. (b) Intensity envelope of the incident IR pulse (blue) and resulting attotrain from H10 to H50 (red). (c) Power spectra of the reflected (red) and the corresponding incident pulses (blue). The shaded area denotes the frequency range H10–H50 for which the AP train in (b) is obtained. (d) Spectrogram of the reflected pulse obtained with a half-laser-cycle long Chebyshev window. (e) Time resolved spectral power density (lineouts at peaks of the spectrogram). −4/3 (green dashed line) and −8/3 (cyan dotted-dashed line) scalings are also shown in (c) and (e). Laser parameters are $a_L = 10$, $\tau_L = 5$ fs, $\varphi_{CEP} = 0.75\pi$; initial plasma scalelength $L = 0.2\lambda_L$; incidence angle $\alpha = 45°$.

the fundamental frequency ω_L ($I_{ref}(\omega)$ red curve in (c)). When a bandpass filter is used to select the 10th to 50th harmonic components, an attosecond pulse train (attotrain) results. This H10-H50 bandpass filter is a constant gate function with the two edges rounded with cosine roll-offs extending two harmonic orders and mimics the transmission window of an aluminum filter. It will be used throughout this paper unless stated otherwise. The attotrain comprises four APs appearing at temporal positions corresponding to the strongest modulations in the reflected electric field (red curve in (b)). The peak intensity of the strongest AP is $I_{AP} = 1.3 \times 10^{21}$ W/cm^2, i.e., 5 times higher than that of the incident pulse (blue curve in (b)), while the corresponding electric field normalized to λ_L is $a_{AP} \simeq 25$. Furthermore, a detailed analysis reveals that the AP near the peak of the laser pulse is 10 times more intense compared to the next strongest AP in the train, although its energy is only five times higher. This is consistent with its relatively short duration of 63 as. The corresponding isolation degree characterizing the *purity* of single AP generation is >10, thus the other APs in the train are barely discernible. The isolation degree is defined here as the intensity ratio between the strongest and second strongest AP in the train. It is interesting to note that, despite the high isolation degree here, clear fringes still appear in the corresponding spectral range H10–H50 of the reflected spectrum. In addition, we observe that the spacing between subsequent AP peaks is decreasing (positive harmonic chirp). Detailed analysis shows that, these clear fringes come from an overall effect of the decreasing temporal spacing of APs in the attotrain and the presence of the much weaker APs. The decreasing temporal spacing of the attotrain is due to the denting of the reflecting electron surface resulting from the strong radiation pressure effect on a finite scale length plasma density profile. It leads to the spectral modulation with period $<10\omega_L$ (see Fig. 1(c)). The decreasing temporal spacing due to the denting of the reflection surface has also been reported by Behmke *et al.*[31] Compared to their results, the spacing changes from one AP to the next for our few-cycle laser pulse case is so large that the spectral amplitude modulation with period $<10\omega_L$ is more significant than the fine structures within one harmonic order. This looks very similar to the spectra reported in the work of Borot *et al.*[32] for similar laser pulse duration and central wavelength, but at a much lower intensity. However, in their work, the modulation structure refers to CWE harmonics and has a different origin, which is the negative harmonic chirp intrinsic to the CWE mechanism.

A more detailed insight in the APG process can be gained by a time-frequency analysis of the reflected electric field with sub-laser-cycle temporal resolution. Fig. 1(d) shows the temporally resolved spectral power density $I_{ref}(\omega, t)$ plot of the reflected pulse. Four vertical stripes can be clearly seen on it, one every laser cycle. It clearly shows that the spectral components of the XUV radiation along these stripes are phase locked, resulting thus in attosecond temporal bunching. Four lineouts at the peak of each stripe are shown in (e) illustrating the dissimilarity of the spectral power density for different APs. The spectrum corresponding to the stripe at $t = 17.43\,T_L$ markedly differs in its structure and clearly dominates over the other contributions. As a result, the corresponding AP (depicted as red curve in Fig. 1(b)) exhibits such a high degree of isolation that one can speak of generating a single AP. In addition, this spectrum has a very shallow roll-off scaling in the spectral range H10–H50, nearly −4/3. This indicates that the emission of the corresponding AP is enhanced by the CSE mechanism.

IV. MULTI-PARAMETER SYSTEMATIC STUDY

For a quantitative evaluation, the attotrain time evolving spectral intensity is integrated to obtain the XUV energy fluence. We distinguish between the train yield $Y_{train} = \int_{\omega_{10}}^{\omega_{50}} \int_{-\infty}^{+\infty} I_{ref}(\omega, t) d\omega dt$ corresponding to the energy fluence for the whole attotrain and that for each AP, i.e., the atto yield $Y_{atto} = \int_{\omega_{10}}^{\omega_{50}} \int_{\Delta t_{stripe}} I_{ref}(\omega, t) d\omega dt$. The train yield is a readily measurable quantity while atto yield characterizes more the physics of the process. To assess whether a single AP is generated under certain conditions, we have to know not only how high is the overall train yield but also how it is distributed among the individual APs of the train, i.e., the atto yield. In our PIC simulations, we find that for $\alpha = 45°$ every laser cycle contains at most one AP, the position of which within the cycle depends on φ_{CEP}. In order to investigate the atto yield distribution within the attotrain, it is convenient to introduce the normalized parameter $\psi_g = (2k\pi + \pi/2 - \varphi_{CEP})/(2\pi\bar{\tau}_L)$. The advantage of this new variable ψ_g is that it combines cycle number and CEP, maintaining thus the information on φ_{CEP} and optical cycle number k but not on the exact temporal

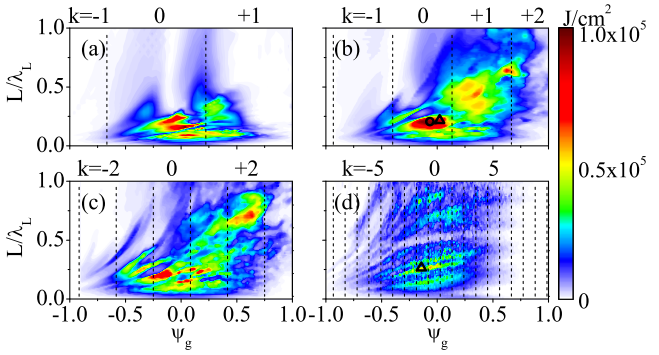

FIG. 2. $\psi_g - L$ plane dependence of atto yield $Y_{\text{atto}}(\psi_g, L)$ at interaction conditions $a_L = 10$ and $\alpha = 45^\circ$ from H10 to H50 for IR driver pulse duration of (a) $\tau_L = 3$ fs, (b) $\tau_L = 5$ fs, (c) $\tau_L = 8$ fs, and (d) $\tau_L = 25$ fs. Hollow circle (hollow triangles) mark(s) out coordinate(s) for the strongest AP(s) in Fig. 1(a) (Figs. 4(a) and 4(b)). Black dashed lines are used to separate the projections of ψ_g from different k. For the definition and interpretation of ψ_g, see text.

location of the AP pulse within the cycle. In the PIC simulations for a given laser pulse duration $\bar{\tau}_L$, the parameters varied are φ_{CEP} and L. Subsequently, for each set of these variables, the obtained atto yield is mapped into $\psi_g - L$ plane. In Fig. 2, the energy fluence $Y_{\text{atto}}(\psi_g, L)$ as a function of ψ_g and L is plotted. As it can be seen, the introduction of the new variable allows to easily ascertain whether an isolated AP or a train is generated and accordingly identify the corresponding regions. It should be noted that this process takes into account the variation of the instantaneous intensity encountered by the *k-th* cycle in the pulse. This way, the different plasma conditions due to spatio-temporally evolving reflection surface, which is closely connected to the laser pulse intensity envelope, are also included.

Another parameter of pivotal importance to the APG process is the scale length L of the expanded plasma layer. It affects the energy coupling process to APG in several ways. It describes whether the layer is "hard" or "soft," affecting the amplitude and temporal evolution of the excited oscillations. Consequently, it influences the matching between the collectively moving electrons and the laser wavefront. It also determines the denting amount of the reflecting electron surface when the peak laser intensity is fixed.[31,33] As a result, it affects the total stored electrostatic energy. In addition, it determines the release rate of electrostatic energy during the emission process when electrostatic field decays due to restoring electrons. The present investigation concentrates on the influence of these two parameters and the laser pulse duration on the APG process for a relevant range of the combined $\psi_g - L$ parameter space.

From one simulation for a specific laser CEP and plasma scale length, the atto yield for several APs in an attotrain can be extracted and projected to the $\psi_g - L$ plane. From a large number of simulations under a systematic variation of CEP and scale length, the two parameter dependence of $Y_{\text{atto}}(\psi_g, L)$ is obtained and shown in Fig. 2 for four driver pulse durations. For the two-cycle driver pulse case ($\tau_L = 5$ fs) in Fig. 2(b), the atto yield contours on $\psi_g - L$ plane are contained primarily in two zones corresponding to $k = 0$ and $k = 1$ laser cycles. The first zone is centered at $\psi_g \approx -0.07$ (i.e., $k = 0$, $\varphi_{\text{CEP}} = 0.75\pi$), $L \approx 0.2\lambda_L$ and it has a width of $\Delta\psi_g \approx 0.42$ (i.e., $\Delta\varphi_{\text{CEP}} \approx 1.58\pi$), $\Delta L \approx 0.15\lambda_L$; while the second zone is centered at $\psi_g \approx 0.36$ (i.e., $k = 1$, $\varphi_{\text{CEP}} = 1.17\pi$), $L \approx 0.43\lambda_L$ and it has a width of $\Delta\psi_g \approx 0.46$ (i.e., $\Delta\varphi_{\text{CEP}} \approx 1.73\pi$), $\Delta L \approx 0.5\lambda_L$. Detailed check shows that the reflected electric field shape from the first zone ($k = 0$) has bipolar structure, while that from the second zone ($k = 1$) has unipolar structure (see Gonoskov *et al.*[26]). This correlates to characteristic time resolved spectrum with and without modulations at the tail correspondingly. The hollow circle in Fig. 2(b) denotes the position of the strongest AP shown in Fig. 1(b). In general, the maximum yield region is located approximately at the center of each of the two zones and is saturated at 1.0×10^5 ($k = 0$) and 0.6×10^5 J/cm^2 ($k = 1$). If we note that the energy fluence of an $a_L = 10$ laser cycle at 0.8 μm is 5.75×10^5 J/cm^2, we can immediately deduce that the XUV conversion efficiency for each of the two laser cycles is higher than 10 percent. In addition, the two zones almost fill the whole $k = 0$ and $k = 1$ areas along ψ_g direction, which indicates a less sensitive CEP dependence of train yield on ψ_g. Moreover, the optimum plasma scale lengths L_{opt} for both zones increase with increasing ψ_g. This suggests that for longer scale lengths, the interacting plasma tends to accumulate potential energy and release it in the form of XUV at a later time. Actually, there exists a sort of resonant scale length L_{opt}, which already has been proven to play an important role in HHG from relativistic laser plasma interactions,[29,31,34] but also a sort of resonant $\psi_{g,opt}$. It becomes clear that the parameters ψ_g and L are correlated with each other exhibiting optimum zones in the $\psi_g - L$ plane. The correlation between ψ_g and L indicates that the laser and plasma conditions have to be matched for efficient emission, which further supports CSE mechanism as explanation for the enhanced atto yields. The resonant $\psi_{g,opt}$ here can be quite off from zero. This is in strong contrast with those cases where only ROM or CWE mechanism is present, as in the work of Borot *et al.*[32] For those cases, no matching between laser and plasma conditions is needed, thus the atto yield should be more or less proportional to laser intensity. We have also checked different spectral windows other than H10–H50 and have found similar XUV yield contours. We generally get higher isolation degrees from higher spectral windows, though.

The role of the laser pulse duration in APG process is depicted in Fig. 2 where the corresponding atto yield contours are shown for one cycle ($\tau_L = 3$ fs) to ten cycles ($\tau_L = 25$ fs) driver pulse durations. The optimum regions in the $\psi_g - L$ plane display an evolution. For the one-cycle case in Fig. 2(a), the contour features several stripes followed by a small continuous area with decreased energy fluence. Optimal scale lengths are limited to $L < 0.4\lambda_L$. For the two-cycle case in Fig. 2(b), those stripes from Fig. 2(a) merge into a broader one and form the first optimum zone mentioned previously. The tiny continuous area from Fig. 2(a) also becomes much broader and forms the second optimum zone. Optimal scale lengths are limited to $L < 0.7\lambda_L$. For the three-cycle case in Fig. 2(c), the optimum region becomes stratified and optimal scale lengths extend to $L < 0.9\lambda_L$. When laser pulses are longer than five cycles (≥ 15 fs), optimal scale lengths extend

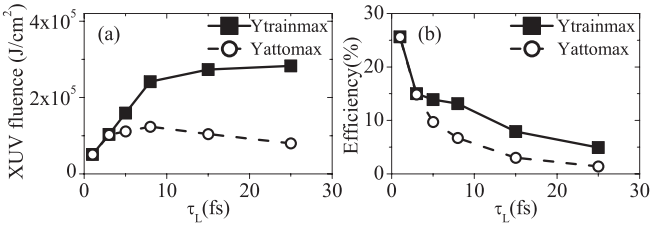

FIG. 3. τ_L dependence of (a) the maximum train yield (black squares) and atto yield (hollow circles) and (b) the maximum train yield efficiency (black squares) and atto yield efficiency (hollow circles) from harmonic orders H10–H50. Interaction conditions are the same as those in Fig. 2.

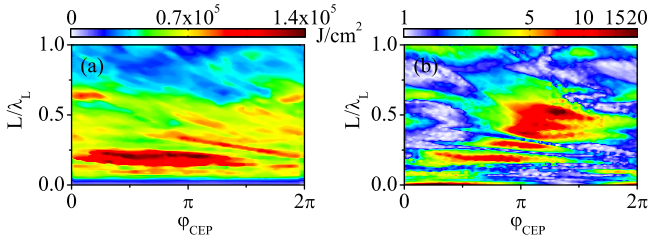

FIG. 5. $\varphi_{CEP} - L$ plane dependence of XUV energy fluence per attotrain (a), and of isolation degree of the strongest AP from the train (b). Interaction conditions are the same as those in Fig. 2(b). H10–H50 are used for synthesizing the APs.

beyond $1\lambda_L$. The shape of the contour stays nearly unchanged within the scale length range $L \leq 1\lambda_L$ and all of the contours look very similar to that showed in Fig. 2(d). The optimum regions encompass two zones, one for $L < 0.5\lambda_L$ and another for $L > 0.5\lambda_L$; each zone itself is very stratified. The atto yields exhibit a weaker scale length dependence and the maximum value also decreases. For the driver pulse durations shown here, the number of APs contained in the optimal region is roughly the number of cycles within the intensity FWHM of the laser pulse. As expected, the shorter the laser pulse duration, the fewer APs are produced in one attotrain. Nevertheless, the optimum region is obviously tilted in the $\psi_g - L$ plane. The yield is more strongly enhanced for shorter scale lengths in the rising edge of the pulse, while the opposite occurs in the trailing edge. This is important especially for few-cycle driver case like the one for the two-cycles shown in Fig. 2(b). Assuming to have control over the CEP of the laser pulse and the scale length of the resulting plasma, this makes it possible, by appropriate choice of these two parameters, to generate a single AP (either in $k = 0$ or $k = 1$ region). For the fixed laser intensity studied here, a two-cycle pulse appears to be the best choice among all the driver pulse durations, because it exhibits a broad and also not so stratified optimum region.

The laser pulse duration dependence of the maximum train Y^{max}_{train} and atto Y^{max}_{atto} yield as well as the corresponding efficiency is summarized in Fig. 3. The maximum train yield shows a rapid increase for $\tau_L \leq 8$ fs; while this increase starts to saturate for $\tau_L > 8$ fs. In the $1\text{ fs} \leq \tau_L \leq 3$ fs range, the maximum atto yield closely follows the maximum train yield, which indicates the generation of a single AP. For the pulse duration range of $5\text{ fs} \leq \tau_L \leq 8$ fs, the maximum atto yield reaches an optimum whereas for $\tau_L > 8$ fs, it decreases. Unexpectedly, the train yield does not significantly change for $\tau_L > 8$ fs. The energy conversion efficiencies for both the maximum train yield and atto yield drop when laser pulse duration increases.

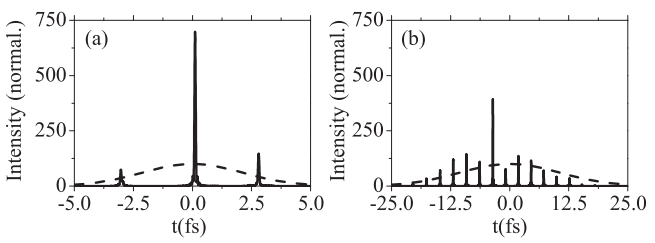

FIG. 4. Intensity envelope of attotrain (solid) and that of its corresponding incident laser pulse (dashed) for the maximum atto-yield and for (a) $\tau_L = 5$ fs and (b) $\tau_L = 25$ fs. Other interaction conditions are $\varphi_{CEP} = 0.42\pi$, $L = 0.21\lambda_L$, and $\alpha = 45°$ for (a); $\varphi_{CEP} = 1.17\pi$, $L = 0.25\lambda_L$, and $\alpha = 45°$ for (b). H10–H50 are used for synthesizing the APs.

This pulse duration dependence of the train and atto yields can be understood by examining the two attotrains in Fig. 4, produced for $\tau_L = 5$ fs and $\tau_L = 25$ fs. In relativistic few-cycle laser plasma interaction, CSE-like energy coupling results in enhancement of the atto yields. From Fig. 4, it can be seen that the degree of enhancement diminishes when the pulse duration becomes longer. In the $\tau_L = 5$ fs case in Fig. 4(a), one AP is amplified to intensities much higher than the incident laser peak intensity as well as all the remaining APs. For $\tau_L = 25$ fs case, a single AP is still predominantly enhanced over all the rest, albeit the peak intensity of the enhanced AP is considerably less compared to that with 5 fs pulse duration. For a few-cycle laser pulse, the atto yield contours exhibit a continuous optimum region, whereas for a many-cycle pulse, the atto yield contours are stratified. This behavior causes the maximum train yield curve in Fig. 3(a) to exhibit a saturation effect for durations $\tau_L > 8$ fs.

V. DISCUSSION AND CONCLUSION

This study was primarily motivated by experiments planned with the state-of-the-art upgraded LWS-20 laser system,[2] which features sub-5 fs and 80 mJ high contrast laser pulses. Using simulation parameters attainable by this laser system, we have calculated the CEP and scale length dependence of train yields expected to be produced. They are shown in Fig. 5(a). In parallel, we have estimated the single AP isolation dependence on the same parameters (see Fig. 5(b)). Notwithstanding appropriate modifications due to multi-dimensional effects,[35] the findings of our simulations indicate that an unrivalled high energy fluence for the strongest single AP of $\sim 10^4$ J/cm^2 is reachable. This corresponds to $\sim 100\,\mu$J in energy per single AP when we assume a $1\,\mu$m^2 source area. Therefore, we can conclude that with this laser system using the technique of scale length and CEP control, $100\,\mu$J level single attosecond pulses comprising >16 eV photons with isolation degree ~ 10 can be attained.

ACKNOWLEDGMENTS

The work was supported by the Munich Centre for Advanced Photonics (MAP), by DFG Project Transregio TR18 and by the Association EURATOM, Max-Planck-Institut für Plasmaphysik. G. M. and W.Y. also acknowledge

the support from the National Natural Science Foundation of China (11304331, 11174303) and the National Basic Research Program of China (2013CBA01504). W.D. also acknowledges the support from a Foundation Blanceflor Boncompagni Ludovisi, née Bildt, Fellowship. A.B. acknowledges the support from the Marie Curie Fellowship EU-FP7-IEF-ALPINE.

[1]F. Tavella, Y. Nomura, L. Veisz, V. Pervak, A. Marcinkevičius, and F. Krausz, Opt. Lett. **32**, 2227 (2007).
[2]D. Herrmann, L. Veisz, R. Tautz, F. Tavella, K. Schmid, V. Pervak, and F. Krausz, Opt. Lett. **34**, 2459 (2009).
[3]T. H. Dou, R. Tautz, X. Gu, G. Marcus, T. Feurer, F. Krausz, and L. Veisz, Opt. Express **18**, 27900 (2010).
[4]J. M. Mikhailova, A. Buck, A. Borot, K. Schmid, C. Sears, G. D. Tsakiris, F. Krausz, and L. Veisz, Opt. Lett. **36**, 3145 (2011).
[5]T. Wittmann, B. Horvath, W. Helml, M. Schätzel, X. Gu, A. Cavalieri, G. Paulus, and R. Kienberger, Nat. Phys. **5**, 357 (2009).
[6]F. Krausz and M. Ivanov, Rev. Mod. Phys. **81**, 163 (2009).
[7]M. Hentschel, R. Kienberger, C. Spielmann, G. A. Reider, N. Milosevic, T. Brabec, P. Corkum, U. Heinzmann, M. Drescher, and F. Krausz, Nature **414**, 509 (2001).
[8]A. Baltuška, T. Udem, M. Uiberacker, M. Hentschel, E. Goulielmakis, C. Gohle, R. Holzwarth, V. Yakovlev, A. Scrinzi, T. Hänsch *et al.*, Nature **421**, 611 (2003).
[9]R. Kienberger, E. Goulielmakis, M. Uiberacker, A. Baltuska, V. Yakovlev, F. Bammer, A. Scrinzi, T. Westerwalbesloh, U. Kleineberg, U. Heinzmann *et al.*, Nature **427**, 817 (2004).
[10]E. Goulielmakis, M. Uiberacker, R. Kienberger, A. Baltuska, V. Yakovlev, A. Scrinzi, T. Westerwalbesloh, U. Kleineberg, U. Heinzmann, M. Drescher *et al.*, Science **305**, 1267 (2004).
[11]P. Tzallas, E. Skantzakis, C. Kalpouzos, E. Benis, G. D. Tsakiris, and D. Charalambidis, Nat. Phys. **3**, 846 (2007).
[12]E. Goulielmakis, M. Schultze, M. Hofstetter, V. S. Yakovlev, J. Gagnon, M. Uiberacker, A. L. Aquila, E. Gullikson, D. T. Attwood, R. Kienberger *et al.*, Science **320**, 1614 (2008).
[13]E. Skantzakis, P. Tzallas, J. Kruse, C. Kalpouzos, and D. Charalambidis, Opt. Lett. **34**, 1732 (2009).
[14]E. J. Takahashi, P. Lan, O. D. Mücke, Y. Nabekawa, and K. Midorikawa, Nat. Commun. **4**, 2691 (2013).
[15]E. Constant, D. Garzella, P. Breger, E. Mével, C. Dorrer, C. Le Blanc, F. Salin, and P. Agostini, Phys. Rev. Lett. **82**, 1668 (1999).
[16]G. Sansone, L. Poletto, and M. Nisoli, Nat. Photonics **5**, 655 (2011).
[17]S. Gordienko, A. Pukhov, O. Shorokhov, and T. Baeva, Phys. Rev. Lett. **93**, 115002 (2004).
[18]G. D. Tsakiris, K. Eidmann, J. Meyer-ter-Vehn, and F. Krausz, New J. Phys. **8**, 19 (2006).
[19]P. Heissler, R. Hörlein, J. M. Mikhailova, L. Waldecker, P. Tzallas, A. Buck, K. Schmid, C. M. S. Sears, F. Krausz, L. Veisz, M. Zepf, and G. D. Tsakiris, Phys. Rev. Lett. **108**, 235003 (2012).
[20]F. Quéré, C. Thaury, P. Monot, S. Dobosz, P. Martin, J.-P. Geindre, and P. Audebert, Phys. Rev. Lett. **96**, 125004 (2006).
[21]R. Lichters, J. Meyer-ter-Vehn, and A. Pukhov, Phys. Plasmas **3**, 3425 (1996).
[22]D. an der Brügge and A. Pukhov, Phys. Plasmas **17**, 033110 (2010).
[23]A. Tarasevitch, K. Lobov, C. Wünsche, and D. von der Linde, Phys. Rev. Lett. **98**, 103902 (2007).
[24]T. Baeva, S. Gordienko, and A. Pukhov, Phys. Rev. E **74**, 046404 (2006).
[25]T. Boyd and R. Ondarza-Rovira, Phys. Lett. A **374**, 1517 (2010).
[26]A. A. Gonoskov, A. V. Korzhimanov, A. V. Kim, M. Marklund, and A. M. Sergeev, Phys. Rev. E **84**, 046403 (2011).
[27]B. Dromey, S. Rykovanov, M. Yeung, R. Hörlein, D. Jung, D. Gautier, T. Dzelzainis, D. Kiefer, S. Palaniyppan, R. Shah *et al.*, Nat. Phys. **8**, 804 (2012).
[28]J. M. Mikhailova, M. V. Fedorov, N. Karpowicz, P. Gibbon, V. T. Platonenko, A. M. Zheltikov, and F. Krausz, Phys. Rev. Lett. **109**, 245005 (2012).
[29]S. Kahaly, S. Monchocé, H. Vincenti, T. Dzelzainis, B. Dromey, M. Zepf, P. Martin, and F. Quéré, Phys. Rev. Lett. **110**, 175001 (2013).
[30]A. Bourdier, Phys. Fluids **26**, 1804 (1983).
[31]M. Behmke, D. an der Brügge, C. Rödel, M. Cerchez, D. Hemmers, M. Heyer, O. Jäckel, M. Kübel, G. G. Paulus, G. Pretzler, A. Pukhov, M. Toncian, T. Toncian, and O. Willi, Phys. Rev. Lett. **106**, 185002 (2011).
[32]A. Borot, A. Malvache, X. Chen, A. Jullien, J.-P. Geindre, P. Audebert, G. Mourou, F. Quéré, and R. Lopez-Martens, Nat. Phys. **8**, 416 (2012).
[33]H. Vincenti, S. Monchocé, S. Kahaly, G. Bonnaud, P. Martin, and F. Quéré, Nat. Commun. **5**, 3403 (2014).
[34]F. Dollar, P. Cummings, V. Chvykov, L. Willingale, M. Vargas, V. Yanovsky, C. Zulick, A. Maksimchuk, A. G. R. Thomas, and K. Krushelnick, Phys. Rev. Lett. **110**, 175002 (2013).
[35]P. Heissler, A. Barna, J. M. Mikhailova, G. Ma, K. Khrennikov, S. Karsch, L. Veisz, I. B. Földes, and G. D. Tsakiris, Appl. Phys. B **118**, 195 (2015).